Experimental measurement of the electron energy distribution function in the radio frequency electron cyclotron resonance inductive discharge

ChinWook Chung*
Department of Electrical and Computer Engineering, HanYang University, Seongdong-gu, Seoul 133-791, Republic of Korea

S. S. Kim
Korea Basic Science Institute, Daejon 305-333, Republic of Korea

H. Y. Chang
Department of Physics, Korea Advanced Institute of Science and Technology, Daejon 305-701, Republic of Korea
(Received 1 April 2003; revised manuscript received 9 September 2003; published 29 January 2004)

Recently, the existence of electron cyclotron resonance (ECR) in a weakly magnetized inductively coupled plasma (MICP) has been evidenced [ChinWook Chung *et al.*, Phys. Rev. Lett. **80**, 095002 (2002)]. The distinctive feature of the ECR effect in the MICP is efficacious heating of low-energy electrons. In the present paper, electron heating characteristics in the MICP have been investigated by observing electron energy distribution function dependencies on various external parameters such as gas pressure, driving frequency, and rf power (electron density). It is found that the ECR effect on electron heating becomes enhanced with decreasing pressure or increasing driving frequency. The ECR heating becomes weak at high rf power due to the electron-electron collisions.

DOI: 10.1103/PhysRevE.69.016406 PACS number(s): 52.80.−s, 52.38.Bv

I. INTRODUCTION

Inductively coupled plasma (ICP) source is one of the promising plasma devices for semiconductor manufacturing and a light source [1]. Many researchers have investigated its heating mechanism and plasma characteristics at low pressure where the collisionless heating mechanism is dominant [2–6]. Two types of ICP reactors are available. They differ by chamber shape and antenna position. One is planar type having a planar coil at the top of the chamber. The other is the solenoidal type having a solenoidal coil wound around the side of the chamber.

To improve ICP characteristics in terms of processing, a weakly magnetized ICP (MICP) was suggested and experimental results indicated that a proper application of a weak external magnetic field to the planar ICP could improve many discharge characteristics of the ICP such as electron heating efficiency, uniformity, plasma potential, and impedance matching [7]. Its application to the oxide etching revealed signs of less damage to the silicon surface with increasing etch rate and selectivity [8].

In terms of plasma physics, the role of the weak magnetic field on ICP characteristics has been theoretically investigated [9]. A few experiments under low magnetic field [10–12] have focused on the effect of Trivelpiece-Gould waves as surface waves on helicon plasma sources. Recently, the existence of electron cyclotron resonance (ECR) in rf inductive discharge is found and its direct evidence through the electron energy distribution function (EEDF) measurement is reported [13]. In Ref. [13], it is observed a significant change in the low-energy range of the EEDF at the ECR condition, indicating the existence of collisionless ECR heating in the MICP. It is noted that not electron density but electron temperature is at a maximum near the ECR condition, which is one of the reasons the rf ECR had not been reported: many researchers had expected that electron density will be at a maximum at the ECR condition [14–18].

As a continuous study, this paper investigates the ECR heating characteristics by measuring the EEDF at various conditions with changing pressure, driving frequency, and rf power. The results show that the heating of low-energy electrons is enhanced with increasing system collisionality ν_{en}/ω. At high rf power (high electron density), the ECR heating becomes weak due to the electron-electron collisions.

II. EXPERIMENTAL APPARATUS

The measurement is made in a planar inductive discharge reactor in Fig. 1. An external Helmholtz coil with an inner diameter of 37 cm and a width of 7 cm is installed to make a dc magnetic field, and the dc magnetic field, having a 5% uniformity within the reactor, is generated up to 50 G. A one-turn copper coil with a diameter of 15 cm is wound upon a pyrex plate of 21 cm in diameter and 1.5 cm thick. The distance between the grounded substrate and antenna is 15 cm. rf power (ENI, model A1000) up to 1000 W with frequencies from 0.3 to 35 MHz can be delivered to the coil through an alternative matching network. The reflected power is monitored and the matching circuit is retuned as necessary to keep the reflection under 1%.

III. THE EEDF MEASUREMENT

A. A single Langmuir probe

A Langmuir probe made of tungsten wire 4 mm long and 0.1 mm in diameter is placed in the center of the chamber ($r=0$ cm and $z=7.5$ cm). As presented in Ref. [19], the probe system consists of a small measurement probe and a

*Electronic address: joykang@hanyang.ac.kr

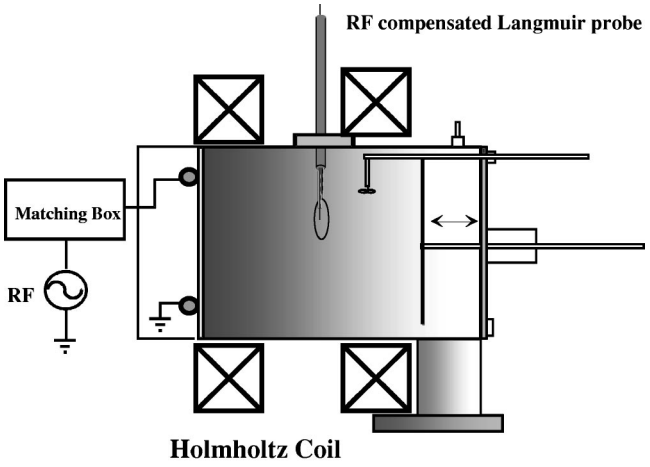

FIG. 1. Sketch of chamber system.

floating-loop reference probe with a resonant filter [20] that reduces rf distortion of the probe characteristics. The effect of the weak magnetic field on the Langmuir probe is negligible because the probe radius is much smaller than electron gyro radius [21]. The probe sweep is done at 1 Hz and the frequency of the superposed signal is 10 kHz with an amplitude less than 0.5 V. Data are averaged in a digital oscilloscope and transferred to a PC through a general purpose interface bus (GPIB).

Electron energy distribution often departs significantly from the Maxwellian in a low-pressure discharge. For example, the electron energy distributions of low-pressure argon CCP [22] and an argon ICP [23] in the *E*-mode are given, which can be approximated by a two-temperature Maxwellian. For a non-Maxwellian and isotropic distribution, a Druyvesteyn analysis for the EEDF measurements is popular and reliable. The second derivative with respect to the probe potential is proportional to the electron energy probability function (EEPF), $g_e(\epsilon)$, and related to the EEDF, $f_e(\epsilon)=\epsilon^{1/2}g_e(\epsilon)$, by the Druyvesteyn formula:

$$f_e(\epsilon)=\frac{2m_e}{e^2A_p}\left(\frac{2eV}{m_e}\right)^{1/2}I_p''(V), \quad eV\equiv\epsilon, \tag{1}$$

where e and m_e are electron charge and mass, respectively, I_p'' is the second derivative with respect to the probe potential, $V=V_p-V_b$ is the probe potential referenced to the plasma dc space potential, and A_p is the surface area of the probe tip. Electron density n_e and effective temperature T_{eff} can be calculated from the EEPF $f_e(\epsilon)$ [24].

For the acquisition of the EEDF, the ac signal superposition method is used [19,25]. The ac superposition technique, which has the advantage of low output noise, is used for the acquisition of the second derivative of the probe characteristic which is proportional to the EEPF. This technique is the method of superposing an ac signal v_{ac} on the probe and detecting a harmonic component corresponding to the derivative. Several techniques of ac signal combinations are available for v_{ac} and the detection frequency component [26]. The measuring circuit and a Langmuir probe system are shown in Ref. [19].

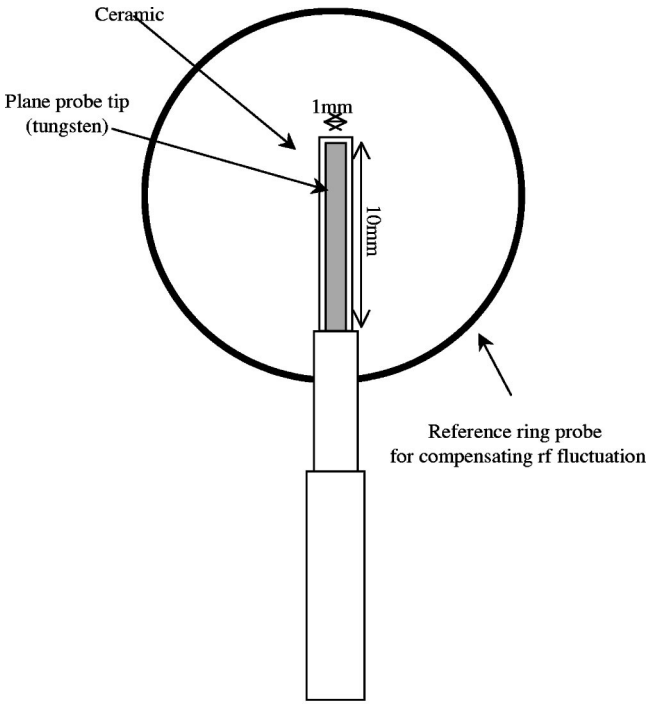

FIG. 2. Sketch of a plane probe.

B. A plane probe

To verify that the EEDF is isotropic at the ECR condition, we measured the EEDF at the same conditions and position of the single Langmuir probe by a plane probe shown in Fig. 2. The plane probe was constructed to measure the EEDF in the parallel and perpendicular directions to the magnetic field. The current to the probe is given as follows:

$$I_e=e\int_{v_{min}}^{\infty}f_\perp(v_\perp)v_\perp dv_\perp, \tag{2}$$

where $v_\perp$ is velocity perpendicular to the probe surface, $f_\perp$ is

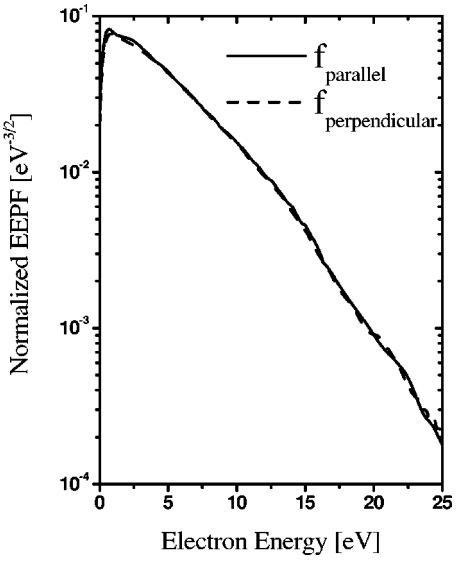

FIG. 3. The EEPFs in both direction (parallel and perpendicular) to the magnetic field (13.56 MHz, 1 mTorr, and 200 W).

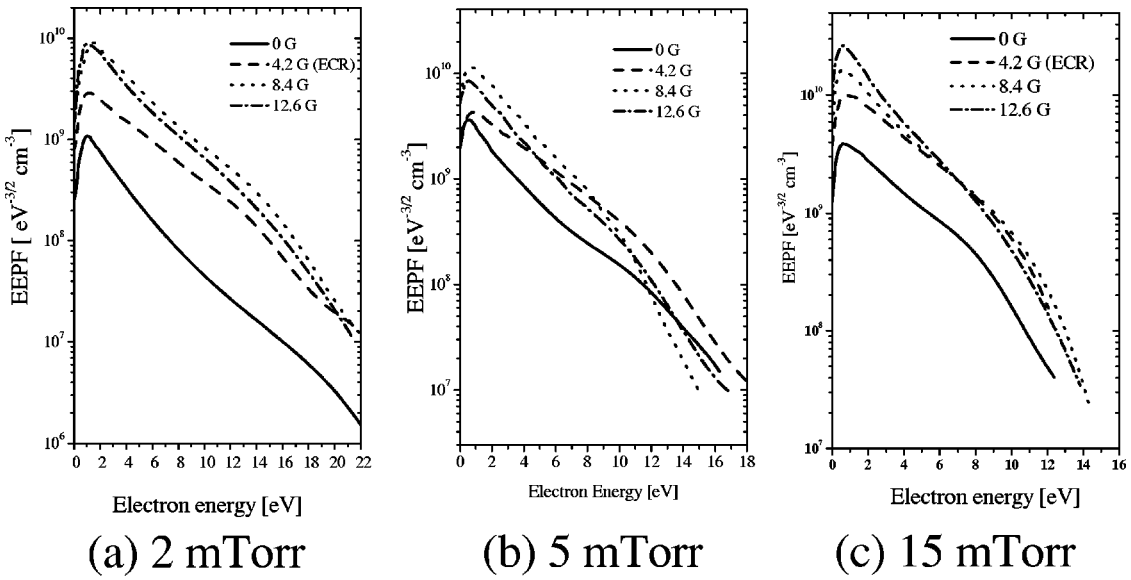

FIG. 4. The pressure dependence of the ECR heating at rf power 150 W. (a) 2 mTorr, (b) 5 mTorr, (c) 15 mTorr.

an electron energy distribution function in the direction perpendicular to the probe surface, and $v_{min} \equiv [2e(V_p - V_{bias})/m_e]^{1/2}$. Thus, we can obtain the energy distribution function by taking the first derivative or the second derivative of I-V curve ($f_\perp \propto dI_e/dV, f_\perp \propto dI_e^2/dV^2$). In fact, in order to properly apply a planar probe to the plasma, a little care is needed. The probe width should be much larger than the sheath for electrons to see the plane probe as an infinite plane and its radius should be smaller than the gyro radius to neglect the magnetic field effect on probe characteristics. We made the planar probe keeping these problems in mind and checked out the probe characteristics during experiment. We obtained the EEPF from the second derivative of the I-V curve and measured it in both orientations to the magnetic field by rotating the probe.

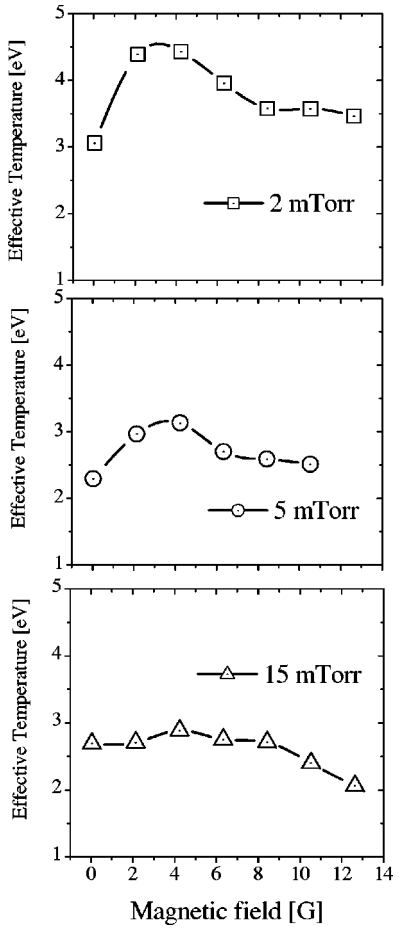

FIG. 5. The effective electron temperatures from Fig. 4.

IV. EXPERIMENTAL RESULTS AND DISCUSSION

A. Isotropy of the EEDF at the ECR

Since the ECR heats electrons in the perpendicular direction to the magnetic field, the EEDF may have some anisotropy at the ECR condition. In order to check out the isotropy of the EEDF, we measured the EEDFs in both (parallel and perpendicular) directions to the magnetic field at the ECR condition using the plane probe. Figure 3 shows the EEPFs measured at very low pressure (1 mTorr) for Ar discharges. As shown in Fig. 3, the EEPFs are nearly identical with each other indicating that the EEDF is isotropic even in the ECR condition.

This isotropization of the EEPF can be explained as collisional relaxation. For the EEDF to be isotropic, the electrons should suffer a large number of collisions within its lifetime $\tau_l = aL/u_B$ (L is chamber length, u_B is Bohm velocity, a is the ratio of density at edge to density at body), which is well-known isotropization criterion [27–29]. Typically, for a weakly ionized plasma electron-neutral (e-n) collisions are dominant collision process of electrons. In our experiment, since the $e-n$ collision frequency $\nu_{en}(\sim 10^7)$ is much higher than τ_l^{-1} ($\sim 10^5$), the isotropization criterion is well satisfied.

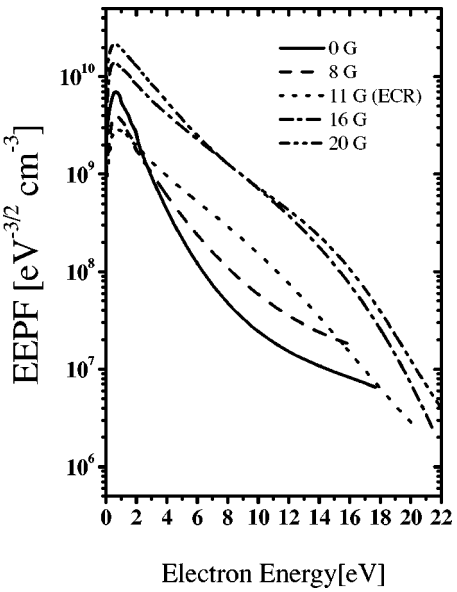

FIG. 6. The EEPF evolution at 30 MHz (argon 2 mTorr, 400 W).

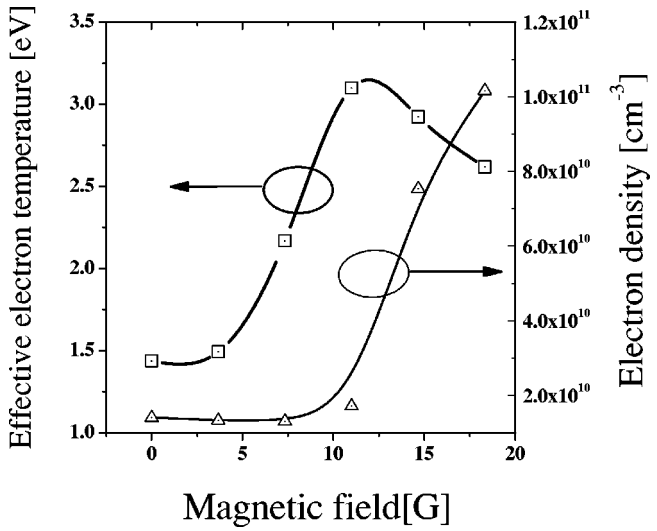

FIG. 7. The electron densities and electron temperature against the magnetic field from the EEPFs of Fig. 6.

B. Pressure effect on the ECR

Figure 4 presents the EEPFs measured at various pressures (2, 5, and 15 mTorr) for Ar discharges when 200 W rf power at 13.56 MHz is applied. The effective electron temperatures obtained from Fig. 4 are given in Fig. 5. In low pressure regime (2 and 5 mTorr), it is observed the depletion of low-energy part of the EEDF near the ECR condition indicating the low-energy electrons are effectively heated by the ECR. As a result, the effective temperature near the ECR increases from 3 to 4.4 eV for 2 mTorr and from 2.2 to 3.6 eV for 5 mTorr in comparison with magnetized cases. For a high pressure (15 mTorr), the ECR effect is not distinctive because of the following two reasons: (1) collisions with neutral atoms break the ECR and (2) low-energy electrons in an ICP without magnetic field are heated more efficiently at higher pressures [30]. The effective electron temperature at 15mTorr is higher than that at 5mTorr, which seems to be unusual in the ICP. But in our ICP system without a Faraday shield, capacitive fields and inductive fields exist simultaneously before the *E-H* transition from the capacitive mode to the inductive mode(low rf power). In inductive mode, the effective temperature is higher at lower pressure [31]. But in the capacitive mode of the ICP, the effective temperature is higher at higher pressure due to the stochastic heating and the Ramsauer effect [32] as in capacitive discharge [22]. Note that the effective temperature at 15 mTorr above 10 G becomes lower than that at 5 mTorr although the temperature at higher pressure is higher at 0 G. This is consistent with Ref. [33] that the mode transition occurs by a magnetic field.

C. Frequency effect on the ECR

Figure 6 shows the measured EEPFs at high driving frequency (30 MHz). In Fig. 7, the effective temperature and the electron density derived from the EEPFs of Fig. 6 are plotted as a function of magnetic field. Overall trends are similar with the lower-frequency case except that the electron density starts to increase from the ECR. The electron temperature, not the electron density, is still at its maximum at the ECR condition. The increase in the effective electron temperature more than doubles (from 1.7 to 3.6 eV) from 0 G to 11 G (ECR). The enhancement of the ECR effect at higher frequency was briefly discussed in Ref. [13]: the electron energy diffusion coefficient derived in the paper shows sharper ECR peak at lower value of ν_{en}/ω (thus at higher frequency under fixed pressure). Its physical origin is dis-

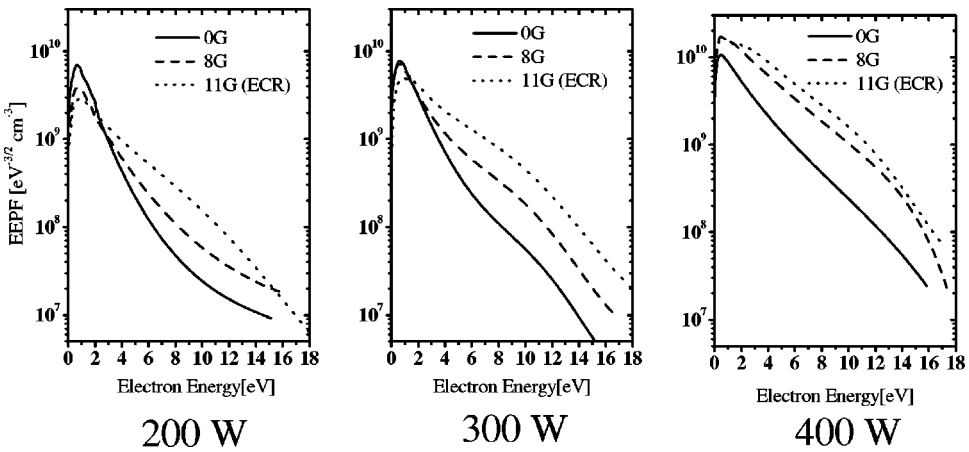

FIG. 8. The EEPF dependence as a function of rf power at 30 MHz and at 2 mTorr.

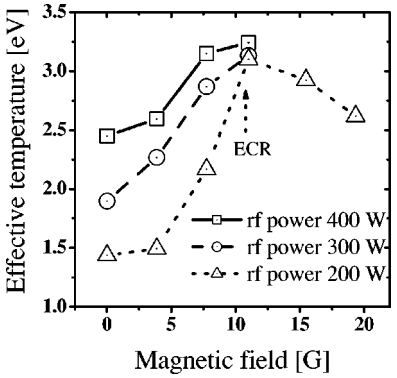

FIG. 9. The effective electron temperatures from the EEPFs in Fig. 8.

cussed in Ref. [30]. When $\nu_{en}/\omega<1$, bounce resonant electrons with axial velocity $v_z^{res,n}=\omega/k_n$ or $|\omega-\omega_{ce}|/k_n$ play an important role in ICP or MICP heating, where $k_n=n\pi/L$ is wave number of the nth Fourier mode of electric field and $\omega_{ce}=eB_0/m_e$ is the electron cyclotron frequency. Slow electrons with velocity v less than $v_z^{res,n}$ are not able to be resonant with the nth mode of electric field and participate in heating in the collisionless case. Since the bounce resonance velocity increases with increasing wave frequency, the number of such inefficient electrons becomes large at high frequency. In this case, the application of magnetic fields reduces the bounce resonance velocity and the number of inefficient electrons decreases remarkably at the ECR condition. This is why the transition of EEDF by the ECR appears more clearly at high frequency.

D. RF power effect on the ECR

Since electron-electron (e-e) collision frequency is proportional to electron density, the electron density is expected to be one of the parameters to affect the ECR. To investigate the density effect, we delivered various rf powers (200, 300, and 400 W) into the plasma. The EEPF power dependence is shown in Fig. 8. The effective temperature from Fig. 8 is given in Fig. 9. The e-e collision frequencies calculated from the Coulomb collision formula ($\nu_{ee}=2.9\times10^{-6}n_eT_e^{-3/2}\ln\Lambda$) [19] in Fig. 10 show that the e-e collision frequency increases with respect to rf power and they do not increase steeply between 200 W and 300 W because of the increase in the temperature. The e-e collision frequency at 200W decreases as the magnetic field increases. This shows that the increase in the electron temperature is mainly caused not by the e-e collisions but the effect of the

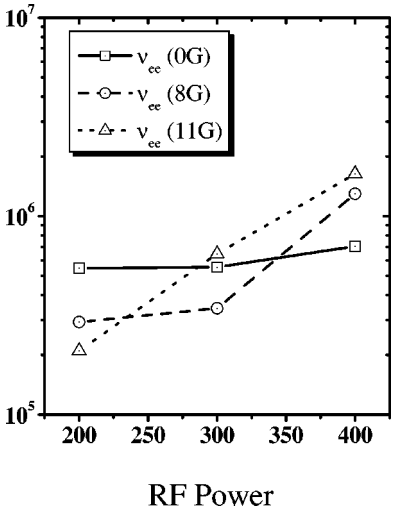

FIG. 10. The electron-electron collision frequency (ν_{ee}) as a function of rf power at various magnetic fields.

magnetic field on electron heating. The EEPFs at 0 G evolve from a bi-Maxwellian distribution to a Maxwellian distribution due to the e-e collision as the rf power goes up. Note that the effective electron temperatures at the ECR are not dependent on rf powers (electron densities) because the electron energy diffusion term by interactions with electric fields is much larger than the diffusion term by the e-e collision at the ECR condition. Due to the e-e collisions, the increase in the effective temperature from 0 G to 11 G (ECR) decreases as the rf power increases and the EEPF transition by the ECR appears more clearly at lower density.

V. CONCLUSION

We checked an anisotropy degree of the EEDF at the ECR condition through a plane probe and in result, the EEPFs are almost isotropic at the ECR. We investigated the ECR heating in a rf inductive discharge at various conditions (pressure, frequency, and rf powers). The ECR heating is very sensitive to pressure and gets weak when the pressure increases. The higher the frequency we applied to the plasma, the stronger the ECR heating. The increase in the effective electron temperature is reduced as rf power goes up.

ACKNOWLEDGMENTS

This work was supported by the SYSTEM I.C. 2010 of Ministry of Science and Technology (MOST) and Ministry of Commerce, Industry, and Energy (MOCIE).

[1] M.A. Lieberman and V.A. Godyak, IEEE Trans. Plasma Sci. **26**, 955 (1998).
[2] V.A. Godyak and V.I. Kolobov, Phys. Rev. Lett. **79**, 4589 (1997).
[3] M.M. Turner, Phys. Rev. Lett. **71**, 1844 (1993).
[4] ChinWook Chung, S.S. Kim, S.H. Seo, H.Y. Chang, and N.S. Yoon, J. Appl. Phys. **88**, 1181 (2000).
[5] ChinWook Chung, K.I. You, and H.Y. Chang, Phys. Plasmas **8**, 2992 (2001).
[6] ChinWook Chung, S.H. Seo, and H.Y. Chang, Phys. Plasmas **7**, 3584 (2000).
[7] H.J. Lee, I.D. Yang, and K.W. Whang, Plasma Sources Sci.

Technol. **5**, 383 (1996).
[8] H.J. Lee, J.H. Kim, K.W. Whang, and J.H. Joo, J. Vac. Sci. Technol. A **14**, 1007 (1996).
[9] S.S. Kim, C.S. Chang, N.S. Yoon, and K.W. Whang, Phys. Plasmas **6**, 2926 (1999).
[10] F.F. Chen, J. Vac. Sci. Technol. A **10**, 1389 (1992).
[11] T. Lho, N. Hershkowitz, J. Miller, W. Steer, and G.H. Kim, Phys. Plasmas **5**, 3135 (1998).
[12] J.E. Stevens, M.J. Sowa, and J.L. Cecchi, J. Vac. Sci. Technol. A **13**, 2476 (1995).
[13] ChinWook Chung, S.S. Kim, and H.Y. Chang, Phys. Rev. Lett. **88**, 095002 (2002).
[14] J. Asmussen, T.A. Grotjohn, P. Mak, and M.A. Perrin, IEEE Trans. Plasma Sci. **25**, 1196 (1997).
[15] S. Matsuv and T. Adachi, Jpn. J. Appl. Phys., Part 1 **21**, 14 (1982).
[16] Y. Weng and M.J. Kushner, J. Appl. Phys. **72**, 33 (1992).
[17] B.-W. Koo, Noah Hershikowitz, and M. Sarfaty, J. Appl. Phys. **86**, 1213 (1999).
[18] V.I. Demidov, S.V. Ratynskaia, R.J. Armstrong, and K. Rypadal, Phys. Plasmas **6**, 350 (1999).
[19] S.H. Seo, C.W. Chung, J.I. Hong, and H.Y. Chang, Phys. Rev. E **62**, 7155 (2000).
[20] V.A. Godyak, R.B. Piejak, and B.M. Alexandrovich, Plasma Sources Sci. Technol. **1**, 36 (1992).
[21] R.R. Arslanbekov, N.A. Khromov, and A.A. Kudryavtsev, Plasma Sources Sci. Technol. **3**, 528 (1994).
[22] V.A. Godyak and R.B. Piejak, Phys. Rev. Lett. **65**, 996 (1990).
[23] S.H. Seo, J.I. Hong, and H.Y. Chang, Appl. Phys. Lett. **74**, 2776 (1999).
[24] M.A. Liberman and A. J. Lichtenberg, *Principles of Plasma Discharges and Materials Processings* (Wiley, New York, 1994).
[25] S.H. Seo, ChinWook Chung, and H.Y. Chang, Surf. Coat. Technol. **131**, 1 (2000).
[26] V.A. Godyak, in *Plasma-Surface Interactions and Processing of Materials*, edited by O. Auciello *et al.* (Kluwer, Dordrecht, The Netherlands, 1990), pp. 95–134.
[27] C.G. Goedde, A.J. Lichtenberg, and M.A. Lieberman, J. Appl. Phys. **64**, 4375 (1989).
[28] V.I. Kolobov, D.P. Lymberopoulos, and D.J. Economou, Phys. Rev. E **55**, 3408 (1997).
[29] U. Kortshagen, C. Busch, and L.D. Tsendin, Plasma Sources Sci. Technol. **5**, 1 (1996).
[30] S.S. Kim, C.W. Chung, and H.Y. Chang, Thin Solid Films **435**, 72 (2003).
[31] V.A. Godyak, R.B. Piejak, and B.M. Alexandrovich, Plasma Sources Sci. Technol. **11**, 525 (2002).
[32] C.W. Chung, and H.Y. Chang, Appl. Phys. Lett. **80**, 1725 (2002).
[33] T. Lho, N. Hershkowitz, J. Miller, W. Steer, and G.H. Kim, Phys. Plasmas **5**, 3135 (1998).